Changes in the Carbon−Carbon and Carbon−Nitrogen Bond Orders in the Macrocycle of Chlorophyll *a* upon Singlet and Triplet Excitation As Probed by Resonance Raman Spectroscopy of Natural-Abundance and Singly and Doubly Labeled Species with ^{15}N, ^{13}C, and ^{2}H Isotopes

Tokutake Sashima,[†] Motoko Abe,[‡] Norihide Kurano,[§] Shigetoh Miyachi,[||] and Yasushi Koyama*,[†]

Faculty of Science, Kwansei Gakuin University, Uegahara, Nishinomiya 662, Japan, Department of Domestic Science, Shoin Women's College, Obanoyama-cho, Shinohara, Nada-ku, Kobe 657, Japan, Marine Biotechnology Institute, Kamaishi Laboratories, 3-75-1 Heita, Kamaishi, Iwate 026, Japan, and Marine Biotechnology Institute, 1-28-10 Hongo, Bunkyo-ku, Tokyo 113, Japan

Received: February 12, 1998; In Final Form: May 6, 1998

The Raman spectra of chlorophyll *a* (1700−1000 cm^{-1}) in the S_0, S_1, and T_1 states were recorded for the species of natural-abundance (NA) isotopic composition and those species that were totally labeled with the ^{15}N, ^{13}C, $^{13}C + {}^{15}N$, ^{2}H, and $^{2}H + {}^{15}N$ isotopes. An empirical normal-coordinate analysis using the S_0 Raman lines of all the isotope species was performed to establish their assignments and to determine a set of force constants including the stretching, bending, nonbonded repulsive force constants and their cross-terms. The C_a-C_m and C_a-N stretching force constants in the S_1 and T_1 states were also determined, on the basis of the assumption that other force constants were the same as those in the S_0 state, to achieve the classification of the observed Raman lines of the NA-, ^{13}C-, and ^{2}H-Chl *a* into two groups: those which shift largely upon the ^{15}N-substitution and are associated with the C_a-N stretching vibrations and those which do not and are associated with the carbon−oxygen and carbon−carbon stretching and the carbon−hydrogen bending vibrations. The resultant stretching force constants were regarded as a scale of the bond orders in the macrocycle in the different electronic states: In the S_0 state, the C_a-C_m bond orders are higher than the C_a-N bond orders, and weak positional dependence is found in both of them. Upon excitation to the S_1 state, the C_a-C_m bond orders decrease, whereas the C_a-N bond orders increase; both of them converge into a single value. Upon excitation to the T_1 state, drastic reorganization of the bond orders takes place in the macrocycle, and the averaged C_a-N bond orders become larger than the averaged C_a-C_m bond orders.

Introduction

The structures of the chlorophyll molecule in the lowest-excited singlet (S_1) and triplet (T_1) states are expected to play key roles in the primary processes of photosynthesis. In bacterial reaction centers (RCs), the S_1-state structure of the special pair bacteriochlorophylls (BChls) is expected to control the initial charge separation.[1] On the other hand, the T_1-state structure of the accessory BChl on the M branch is expected to control the transfer of the triplet energy from the special pair to the carotenoid to be dissipated.[2] Similar organization of the chlorophyll molecules is now being elucidated in the photosystem-I RC of a cyanobacterium, *Synechococcus elongatus*,[3] and in the photosystem-II RC of spinach.[4] In the conjugated system of the macrocycle, the electronic structure and the molecular geometry must be linked closely with each other, and therefore, the excited-state structures must influence strongly the overlap of the LUMO's and HOMO's between a pair of neighboring molecules that are involved in the above charge separation and chlorophyll-to-carotenoid triplet-energy transfer. Changes in the electronic and molecular structure of the macrocycle, upon singlet and triplet excitation, have been predicted theoretically for such model compounds as magnesium chlorin,[5] ethyl chlorophyllide *a*,[6] and ethyl bacteriochlorophyllide *a*.[7] However, little information concerning the excited-state structures has been obtained on the experimental bases.

Transient resonance-Raman spectroscopy has been proved to be a powerful technique in probing the excited-state structures of the conjugated systems in retinoids, carotenoids and chlorophylls.[8] The frequencies of stretching vibrations generally reflect the bond orders of the relevant bonds in the conjugated systems. After the normal-coordinate analysis of the Raman spectra of the unlabeled and the variously isotope-labeled Chl *a*, the bond orders of the conjugated bonds can be measured as a set of stretching force constants. A typical example of this method is T_1-state retinal;[9] in this compound, "the triplet-excited region" where large changes in the carbon−carbon bond orders take place has been determined in terms of a set of stretching force constants.

Transient resonance-Raman spectroscopy has been applied to excited-state bacteriochlorophyll *a* (BChl *a*),[10−13] and characterization of the Raman lines based on spectral comparison among the unlabeled and the ^{15}N- and ^{2}H-labeled BChl *a* in the S_0, S_1, and T_1 excited states and of BChl $a^{+\bullet}$ in the D_0 state lead us to the conclusion that the bond orders of the C_a-C_m

[†] Kwansei Gakuin University.
[‡] Shoin Women's College.
[§] Marine Biotechnology Institute, Kamaishi.
[||] Marine Biotechnology Institute, Tokyo.
* Corresponding author. Phone: 81-798-54-6389. Fax: 81-798-51-0914. E-mail: ykoyama@kgupyr.kwansei.ac.jp.

S1089-5647(98)01118-3 CCC: $15.00
Published on Web 08/11/1998

and the C_a-C_b bonds with a double-bond character decrease, whereas the bond orders of the C_a-N bonds with a single-bond character increase in the following order: the S_0, D_0, T_1, and then S_1 states.[10,11,14,15] Application of transient-Raman spectroscopy to chlorophyll *a* (Chl *a*) is still limited in number. The S/N ratios in the first set of recordings of T_1 Chl *a* were still too low for a detailed analysis,[16] and their spectral patterns were slightly different from the time-resolved Raman spectra with a higher S/N ratio reported later.[17] Neither an authentic T_1 Raman spectrum nor an S_1 Raman spectrum of Chl *a* has been reported since then.

In the present investigation, we recorded the Raman spectra of Chl *a* in the S_0, S_1, and T_1 states for the species of natural-abundance (NA) isotopic composition ("NA-Chl *a*") and those species totally labeled with the ^{15}N, ^{13}C, $^{13}C + ^{15}N$, ^{2}H, and $^{2}H + ^{15}N$ isotopes [^{15}N-, ^{13}C-, ($^{13}C + ^{15}N$)-, ^{2}H-, and ($^{2}H + ^{15}N$)-Chl *a*]. We performed an empirical normal-coordinate analysis using all the S_0 Raman data of the NA-Chl *a* and the above isotope-labeled Chl *a* in order to determine a set of force constants including Urey−Bradley−Shimanouchi (UBS) type force constants and non-UBS cross-terms. We also tried to determine the C_a-C_m and the C_a-N stretching force constants in the S_1 and T_1 states. On the basis of the force constants thus obtained, we are going to answer the following two specific questions: (1) What kind of changes in the bond orders take place in the chlorin skeleton of Chl *a* upon singlet and triplet excitation? (2) How do these changes in the bond orders compare with, or contrast to, those of other cyclic conjugated systems including BChl *a* and metal octaethylporphyrins and octaethylchlorins and those of the linear conjugated systems including retinoids and carotenoids?

Experimental Section

Sample Preparations. NA-Chl *a* was extracted from spinach by a method modified from that of Omata and Murata:[18] Three volumes of acetone was added to spinach leaves after a freeze-and-thaw treatment, and the mixture was homogenized by a blender for 30 s at 0 °C and filtrated. Then $^1/_7$ volumes of a mixture of 1,4-dioxane and water (1:1) were added to the filtrate, and the mixture was left to stand at 0 °C for 10 min. The crystals of Chl *a*−dioxane complex thus formed were spun down and dissolved in ethanol, and the solution was evaporated to dryness. Crude Chl *a* thus obtained was purified by molecular-sieve chromatography using Sepharose CL-6B as adsorbate and 2-propanol/*n*-hexane (1:19) as eluent. The epimer (Chl *a*′) and small amounts of degradation products were then removed by high-pressure liquid chromatography (HPLC) using a silica gel (LiChrosorb Si-60) column (4 mm Φ × 300 mm) and eluent 20% acetone in *n*-hexane.

^{15}N- and ^{13}C-Chl *a* were obtained from the cells of *Chlamydomonas reinhardtii* C-9, which were grown in the tris-acetate-phosphate medium;[19] 400 mg of natural-abundance NH_4Cl in the medium of 1 L was replaced by 500 mg of $(^{15}NH_4)_2SO_4$ for culturing ^{15}N-labeled cells, whereas 1.0 mL of natural-abundance glacial acetic acid was replaced by 1.0 g of $^{13}CH_3{}^{13}COONa$ for culturing ^{13}C-labeled cells. No adaptation of the cells to the isotope-substituted media was necessary. ^{15}N- and ^{13}C-Chl *a* were extracted from the cells and purified in a method similar to that described above. On the other hand, ^{2}H-Chl *a* was extracted from the cells of *Chlorella* sp. WT-1, which were grown in the $^{2}H_2O$-substituted Myers' C Medium[20] in Chlorella Industries, Inc. and purified by the same method. Doubly labeled species, ($^{13}C + ^{15}N$)- and ($^{2}H + ^{15}N$)-Chl *a*, were gifts from the company. Each Chl *a* exhibited a single peak in HPLC when detected at 460 nm; no Chl *a*′ was detected.

S_0 Raman Measurements. S_0 Raman spectra were recorded in ethanol solution (5×10^{-4} M) by the use of the CW 457.9 nm line (20 mW) from an Ar^+-laser (Lexel 95). The sample solution (20−30 mL) was spouted from a nozzle as a flat jet stream (linear speed, ∼0.9 m/s) and circulated to minimize the effect of sample degradation. The optical geometry was as follows: The direction of the stream was horizontal and formed 45° with respect to the optical axis of the spectrometer, and the plane of the jet stream was inclined by 60° with respect to the vertical axis; the probe beam hit the jet plane vertically upward, and the reflected beam propagated downward on the spectrometer side. A 90° Raman scattering was collected and focused onto the slit of a spectrometer (Jasco TRS-300), which was equipped with an image-intensified diode-array detector (Princeton Instruments IRY-700). Spectral data were accumulated in 660 s. The purity of each sample after the Raman measurement (including a trace of Chl *a*′ having the same spectroscopic properties) was determined by HPLC (detection, 460 nm) as follows: NA, 79%; ^{15}N, 96%; ^{13}C, 80%; $^{13}C + ^{15}N$, 93%; ^{2}H, 98%; $^{2}H + ^{15}N$, 99%.

S_1 Raman Measurements. S_1 Raman spectra were recorded in benzene solution (5×10^{-3} M) because ethanol solution gave rise to high fluorescence background. Benzene was used without drying, and therefore, the electronic absorption spectrum of the solution showed no indication of aggregation; further, its ^1H NMR spectrum exhibited no indication of aggregation except for the ^1H signals to be assigned to the phytyl chain and the methyl ester group (data not shown). Each sample solution was sealed in an ampule which was used as a spinning cell; its bottom surface was aligned in the same geometry as the jet plane described above. A one-color experiment was performed by the use of the 390 nm pulses (duration, 50 ps; power, 30 μJ/pulse; repetition, 1 kHz) from a Raman shifter (the first Stokes Raman line from flowing cyclohexane), which was pumped by the TH (351 nm) from a combination of a ML Nd:YLF laser (Quantronix 4216) and a Nd:YLF regenerative amplifier (Quantronix 4417). The photon density was changed, and the difference spectrum of a high-power spectrum (focused) minus a low-power spectrum (defocused) was taken, data accumulation being 660 s. The purity of each sample after the Raman measurement was as follows: NA, 96%; ^{15}N, 92%; ^{13}C, 76%; $^{13}C + ^{15}N$, 83%; ^{2}H, 70%; $^{2}H + ^{15}N$, 97%.

T_1 Raman Measurements. T_1 Raman spectra were recorded in ethanol solution (5×10^{-4} M) by means of a one-color experiment using high and low photon densities as well as by two-color experiments using a pair of pump and probe pulses. In the one-color experiment, a T_1 Raman spectrum was obtained as the difference of a spectrum measured by irradiation of a focused beam minus a spectrum measured with a defocused beam. In the two-color experiment, on the other hand, a T_1 Raman spectrum was obtained as the difference spectrum of a with-pump spectrum minus a without-pump spectrum. The same type of optical geometry as described above was used; the pumping beam in the latter was set coaxial (the same direction) to the probe beam.

(a) One-Color Method Using the 457.9 nm Pump-and-Probe Pulses for the Transient-Raman Measurement of NA-Chl a. The 457.9 nm pulses (pulse duration, 5 ns; power, 2 mJ/pulse; repetition, 10 Hz) from a dye laser (Lambda Physik FL-3003; dye, Coumarin 2), which was pumped by a Nd:YAG laser (Lumonics HY-400), were used for both pumping and probing, data accumulation being 396 s.

(b) Two-Color Method Using the 415 nm Pump and 457.9 nm Probe Pulses for a Set of Time-Resolved Measurements of

NA-Chl a. The 415 nm, SH pulses (pulse duration, 4 ns; power, 0.5 mJ/pulse; repetition, 10 Hz) from a Ti:sapphire laser (CF122L), which was pumped by a Nd:YAG laser (Spectron SL284G), were used for pumping, and the 457.9 nm pulses described above were used for probing. Each probing pulse was delayed electronically in reference to the pumping pulse (0, 20, 50, and 500 ns) by the use of a delayed-pulse generator (Stanford Research Systems DG-535), jitter being ±10 ns. Data accumulation, 396 s.

(c) Two-Color Method Using the 436 nm Pump and 457.9 nm Probe Pulses for NA-Chl a and Isotope-Labeled Chl a; A Fixed (50 ns) Delay Time. The 436 nm pulses from a Raman shifter (H_2, first anti-Stokes), which was pumped by the SH of a Nd:YAG laser (Spectron SL284G), were used for pumping, and the above 457.9 nm pulses were used for probing. The probe pulse was delayed by 50 ns in reference to the pump pulse, and a gate of 80 ns was opened at the delay time of 30 ns to activate the detector by the use of the above delayed-pulse generator and a high-voltage pulse generator (Princeton Instruments FG-100). Data accumulation, 396 s. The purity of each sample after the Raman measurement using method c was as follows: NA, 97%; ^{15}N, 53%; ^{13}C, 77%; ^{13}C + ^{15}N, 95%; ^{2}H, 100%; ^{2}H + ^{15}N, 99%.

Calculations of Normal Vibrations. Figure 1a shows the chemical structure of Chl *a* and the typification of the rings and the carbon atoms in the macrocycle, and Figure 1b shows a model that was used in the calculations of normal vibrations. The following simplifications were made in this model: (1) The 8^2 methyl group was replaced by a mass unit with an atomic weight of 15. (2) Each of the 18^1 methyl, the 17^1 methylene, and the 13^3 carboxyl groups was replaced by a hydrogen atom. (3) The carbon atoms in the macrocycle, those directly attached to it, and those in the vinyl group were assumed to be in the same plane. (4) Concerning the chlorin skeleton, C_{2v} symmetry around the axis connecting the ring II and ring IV nitrogen atoms was assumed. (5) The carbon−oxygen, the carbon−carbon and the carbon−nitrogen bond lengths were taken from the results of X-ray crystallography of ethyl chlorophyllide *a*[21] and modified to satisfy the above symmetry conditions. (6) The C−H bond lengths concerning the olefinic and the paraffinic Hs were assumed to be 1.08 and 1.095 Å, respectively.

The normal vibrations were calculated by Wilson's GF-matrix method using a modified UBS force field; non-UBS cross-terms were also introduced. Programs BGLZ and LSMB, which had been originally written in Prof. Takehiko Shimanouchi's laboratory,[22] were run on a DEC AlphaServer 2100 computer at the Faculty of Science, Kwansei Gakuin University.

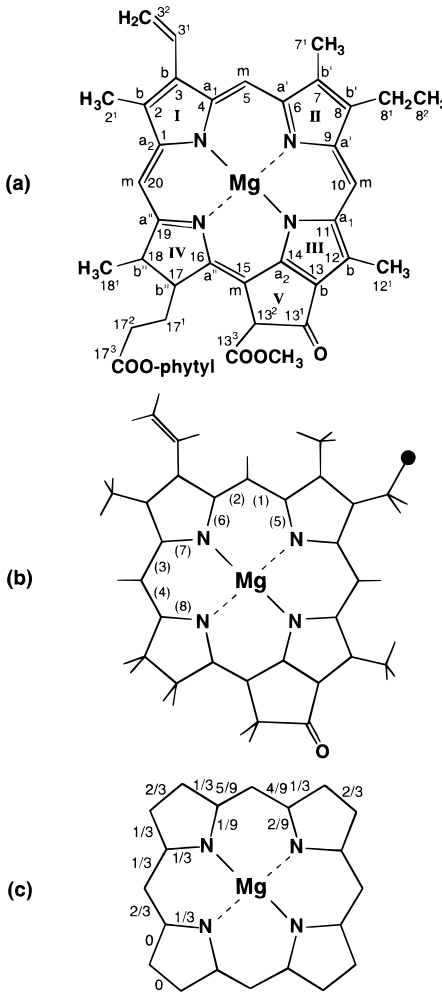

Figure 1. (a) Chemical structure of chlorophyll *a* (Chl *a*) and typification of the five-membered rings and the carbon atoms. (b) A model of Chl *a* used in the calculations of normal vibrations, the details of which are explained in the Experimental Section. The numbering of the C_a-C_m and C_a-N stretching force constants is also shown. (c) An estimation of π-bond orders based on the resonance structures of the chlorin skeleton; each fraction indicates the probability of finding a double bond on the particular carbon−carbon or carbon−nitrogen bond in the set of nine resonance structures.

Results

The T_1 Raman Spectrum of NA-Chl *a*. The first "T_1" Raman spectrum of Chl *a*, which was reported by Nishizawa et al.,[16] showed a sharp, strong line around 1565 cm^{-1}, whereas the T_1 Raman spectrum with a higher S/N ratio, which was reported later by Kanzaki et al.,[17] did not exhibit such a pronounced peak. To obtain an authentic T_1 Raman spectrum, it was necessary to examine this discrepancy in more detail. Figure 2 compares a set of transient Raman spectra including (a) a transient Raman spectrum that was obtained by the one-color method using the 457.9 nm nanosecond pulses and transient spectra that were obtained by the two-color method using the 415 nm pump and the 457.9 nm probe pulses at the delay times of (b) 0, (c) 50, and (d) 500 ns. Comparison of the transient Raman spectra reveals that a sharp 1563 cm^{-1} Raman line on the top of a broad profile can be detected only when the pump and the probe pulses were applied simultaneously (spectra a and b). We speculate that the sharp 1563 cm^{-1} Raman line originates from the second-lowest triplet (T_2) state, because the ab initio calculation of ethyl chlorophyllide *a* by Petke et al.[6] predicted the presence of the T_2 level just below the S_1 level. It is to be noted that this sharp peak was not detected by another pump and probe method using a triplet sensitizer.[16]

In the time-resolved Raman measurement at the "0 ns" delay time shown in Figure 2b, the 436 nm pump pulses could not be used because of their spectral interference, although they were much more efficient for excitation than the 415 nm pulses. Since the spectral interference could be avoided by setting the delay time to 50 ns and by gating the detector in the period of 30−110 ns, we decided to use the two-color method using the 436 nm pump and the 457.9 nm probe pulses in order to obtain pure T_1 Raman spectra for all of the NA-Chl *a* and the isotope-labeled Chl *a*.

Characterization of the S_0, S_1 and T_1 Raman Spectra. *(a) A General Consideration of the Normal Modes.* Before characterizing the S_0, S_1, and T_1 Raman spectra and before starting the normal-coordinate analysis of the observed Raman

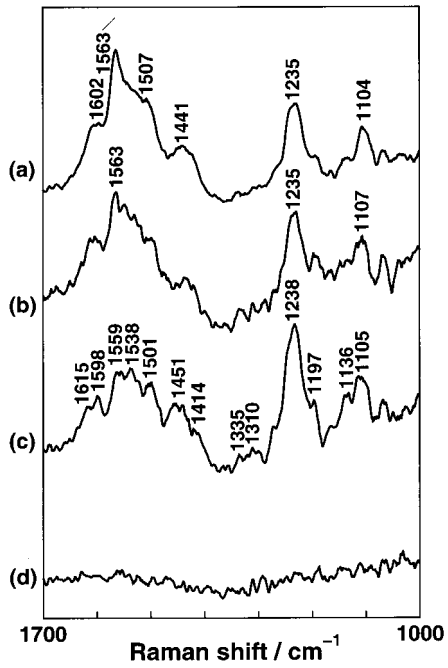

Figure 2. Triplet Raman spectra of NA-Chl *a*. (a) The difference spectrum of a high-photon density spectrum minus a low-photon density spectrum, which were obtained by the one-color method using the 457.9 nm pulses, (b) the difference spectrum of a pump-and-probe spectrum (delay, "0 ns") minus a probe-only spectrum, which were obtained by the two-color method using the 415 nm pump and the 457.9 nm probe pulses, and (c) and (d) the same type of difference spectra, the delay time being 50 and 500 ns, respectively. The sharp peak at 1563 cm^{-1} in spectra a and b is ascribed to the T_2 state, and the rest of the Raman lines in spectrum c are ascribed to the T_1 state.

lines, it was necessary to obtain a general concept of the normal modes of Chl *a*, because the structure of this molecule is complicated and the number of observed Raman lines was limited.

First, we tried to estimate the order in bond order for all the carbon−carbon and carbon−nitrogen bonds in the macrocycle on the bais of the following considerations:

(1) Figure 1c extracts the chlorin skeleton, where nine resonance structures can be drawn by changing the positions of the double bonds (the resonance structures not shown). The number beside each chemical bond indicates the probability of finding a double bond in the set of resonance structures. Assuming that the weight of each resonance structure is equal, the following order in π bond order is expected: $C_{b'}-C_{b'}$, C_b-C_b, and $C_{a''}-C_m$ (probability 6/9 = 2/3); $C_{a1}-C_m$ (5/9); $C_{a'}-C_m$ (4/9); $C_{a2}-C_m$, $C_{a'}-C_{b'}$, $C_{a1}-C_b$, $C_{a2}-C_b$, $C_{a2}-N$, and $C_{a''}-N$ (1/3); $C_{a'}-N$ (2/9); $C_{a1}-N$ (1/9). Hereafter, we will classify the above bonds into four groups (see Figure 1a), i.e., the "C_b-C_b" bonds (including $C_{b'}-C_{b'}$ and C_b-C_b bonds), the "C_a-C_m" bonds ($C_{a'}-C_m$, $C_{a1}-C_m$, $C_{a2}-C_m$, and $C_{a''}-C_m$ bonds), the "C_a-N" bonds ($C_{a'}-N$, $C_{a1}-N$, $C_{a2}-N$, and $C_{a''}-N$ bonds), and the "C_a-C_b" bonds ($C_{a'}-C_{b'}$, $C_{a1}-C_b$, and $C_{a2}-C_b$ bonds); the $C_{a''}-C_{b''}$ and $C_{b''}-C_{b''}$ bonds will be classified into "carbon−carbon single bonds" together with the carbon−carbon bonds in ring V. The stretching vibrations of these bonds in each group are expected to be strongly coupled. Then, the order in bond order can be summarized in terms of the groups of bonds as follows: the C_b-C_b bonds ≥ the C_a-C_m bonds ≥ the C_a-N bonds ≈ the C_a-C_b bonds.

(2) The ab initio calculation of magnesium chlorin predicted the π-bond orders in the S_0 state as follows:[5] C_b-C_b (0.822) > $C_{b'}-C_{b'}$ (0.811) > $C_{a''}-C_m$ (0.645) > $C_{a1}-C_m$ (0.616) > $C_{a2}-N$ (0.605) > $C_{a''}-N$ (0.600) > $C_{a'}-N$ (0.580) > $C_{a'}-C_m$ (0.563) > $C_{a1}-N$ (0.542) > $C_{a2}-C_m$ (0.539) > $C_{a'}-C_{b'}$ (0.424) > $C_{a2}-C_b$ (0.414) > $C_{a1}-C_b$ (0.406). The order may be roughly grouped as follows: the C_b-C_b bonds > the C_a-C_m bonds ≈ the C_a-N bonds > the C_a-C_b bonds.

(3) The stretching force constants of Ni−octaethylporphyrin (Ni-OEP), i.e., $K(C_b-C_b)$, $K(C_a-C_m)$, $K(C_a-N)$, and $K(C_a-C_b)$, were determined by Abe et al.[23] to be 5.89, 5.50, 4.45, and 3.85 mdyn·Å^{-1}, respectively, and by Li et al.[24] to be 7.12, 6.98, 5.64, and 5.43 mdyn·Å^{-1}, respectively. Then, the order in bond order turns out to be the C_b-C_b bonds > the C_a-C_m bonds > the C_a-N bonds > the C_a-C_b bonds in both cases.

All the above considerations lead us to the conclusion that the order in bond order should be as follows: the C_b-C_b bonds ≥ the C_a-C_m bonds ≥ the C_a-N bonds ≥ the C_a-C_b bonds. This order was always taken into account in the normal-coordinate analysis to determine the set of force constants in the S_0 state.

Second, we assumed a symmetry to reduce the number of stretching force constants to be determined: Figure 1a shows that the chlorin skeleton has a C_{2v} symmetry with respect to the axis connecting the ring II and ring IV nitrogen atoms when ring V is excluded; therefore, we assumed that a pair of force constants on both sides of this axis should be the same. Hereafter, we will regard the macrocycle of Chl *a* consisting of all the five rings has "pseudo C_{2v}" symmetry. Actually, the carbon−carbon and carbon−nitrogen bond lengths in the macrocycle of ethyl chlorophyllide *a* dihydrate, whose structure has been determined by X-ray crystallography,[21] do not exhibit this symmetry at all. Therefore, the "pseudo C_{2v} symmetry" is a pure assumption to reduce the number of independent parameters. However, this assumption is convenient to describe the normal modes, because the formation of a pair of in-phase and out-of-phase vibrations with respect to the pseudo C_{2v} axis is expected; the former should appear strongly, whereas the latter should appear weakly in a Raman spectrum.

The normal modes can be characterized differently depending on the relative values of the stretching force constants that belongs to the same group; the following two extreme cases can be expected to take place: When these force constants are almost identical, the unit vibrations within each group can couple strongly with one another even though they are geometrically far apart, and as a result, a limited number of symmetrically coupled modes should give rise to high Raman intensity; asymmetric modes should be very weak. On the other hand, when the force constants are completely different from one another, the vibrations couple only weakly and a set of localized normal modes should give rise to many Raman lines with slightly different frequencies and with comparative intensities.

The following additional characteristics in the normal modes stem from the particular molecular structure of Chl *a* (Figure 1a): (1) The stretching vibrations in the 1700−1000 cm^{-1} region are expected to take place from the higher to the lower frequencies in the following order: the carbonyl C═O stretching, the vinyl C═C stretching, the C_b-C_b, C_a-C_m, C_a-N, and C_a-C_b stretchings in the chlorin skeleton, and the carbon−carbon stretchings in rings IV and V. (2) The C_m-H and the vinyl C−H ip deformation vibrations can couple with the neighboring carbon−carbon stretching vibrations. (3) Under the resonance condition with the Soret $\pi-\pi^*$ transition, those in-plane (ip) vibrational modes that take place in the conjugated system (including the chlorin skeleton, the vinyl group, and the keto carbonyl group) are expected to appear strongly, whereas the ip vibrational modes of the peripheral groups are expected

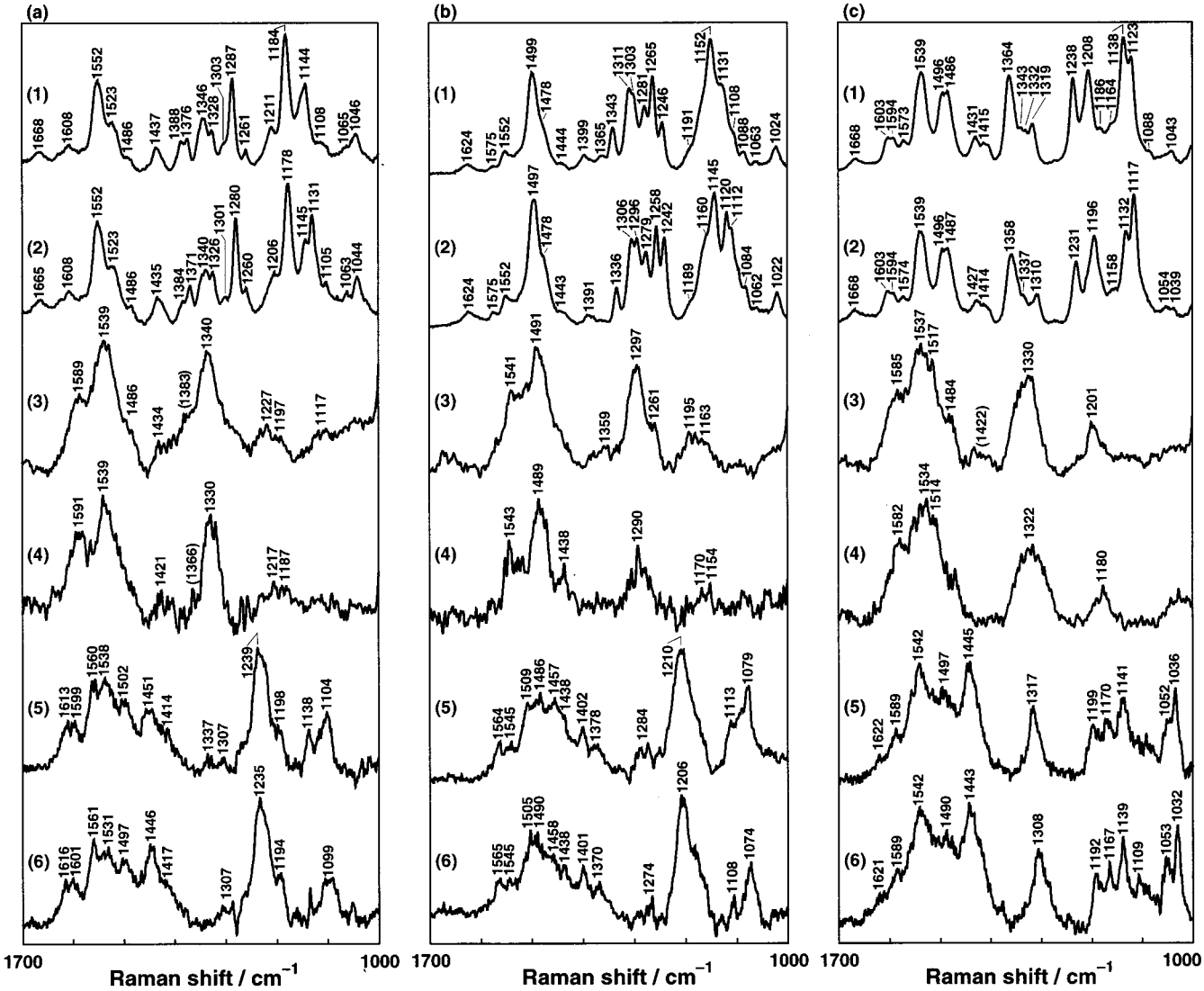

Figure 3. Raman spectra of (a) NA- and ^{15}N-, (b) ^{13}C- and (^{13}C + ^{15}N)-, and (c) ^{2}H- and (^{2}H + ^{15}N)-Chl *a* in the (1), (2) S_0, (3), (4) S_1 and (5), (6) T_1 states. The S_0 Raman spectra were recorded by the CW 457.9 nm beam; the S_1 Raman spectra were recorded by the one-color method using the 390 nm, 50 ps pulses; and the T_1 Raman spectra were recorded by the two-color method using the 436 nm pump and the 457.9 nm probe pulses, delay being 50 ns.

to appear weakly in the resonance-Raman spectrum. Out-of-plane modes are expected to be extremely weak especially in this spectral region.

(b) Characterization of the S_0 Raman Spectra. Parts a-1 and a-2 of Figure 3 show the S_0 Raman spectra of NA- and ^{15}N-Chl *a*. A large number of Raman lines appear in the spectra, a result that suggests that the force constants in each of the groups are different from one another. Table 1 (left) lists the S_0 Raman frequencies of NA- and ^{15}N-Chl *a*: the shifts upon the ^{15}N-substitution are shown in parentheses. A comparison of the shifts leads us to the classification of the Raman lines into two groups: those that shift largely upon the ^{15}N-substitution and those that do not. The chemical structure of Chl *a* (Figure 1a) shows that the former Raman lines should be mainly associated with the C_a-N stretchings, whereas the latter Raman lines with the carbon−oxygen stretching, the carbon−carbon stretchings, or the carbon−hydrogen ip bendings. On the basis of this criterion and the considerations of the normal modes in the previous subsection, the 1668, 1608, and 1552 cm^{-1} Raman lines can be associated with the C═O, C_b-C_b, and C_a-C_m stretchings, respectively, whereas the 1346, 1287, 1184, and 1144 cm^{-1} Raman lines can be associated with the C_a-N stretchings, for example. Since the $^{14}N \rightarrow {}^{15}N$ substitution affects the patterns of normal modes only slightly, it is useful to characterize the Raman lines in this way.

Parts b-1 and b-2 of Figure 3 show the S_0 Raman spectra of ^{13}C- and (^{13}C + ^{15}N)-Chl *a*. Upon the ^{13}C-substitution, the carbon−carbon stretching vibrations shift largely to the lower frequencies, whereas the carbon−nitrogen stretching vibrations shift less. Although the Raman lines become crowded in the lower-frequency region, the general spectral pattern in NA-Chl *a* is conserved. Parts c-1 and c-2 of Figure 3 show the S_0 Raman spectra of ^{2}H- and (^{2}H + ^{15}N)-Chl *a*. In NA-Chl *a*, the C_m-H and the vinyl C−H ip bendings as well as the methyl ip deformation vibrations are originally present in the 1550−1100 cm^{-1} region and push, through coupling, the C_a-C_m stretchings to the higher frequencies, and the C_a-N stretchings to the lower frequencies. Upon the ^{2}H-substitution, those bending and deformation vibrations shift below 1200 cm^{-1}, and as a result, the carbon−carbon and carbon−nitrogen stretching vibrations, which are differently coupled with the carbon−deuterium bending and deformation vibrations, are expected to appear in the 1200−1000 cm^{-1} region.

Table 1 lists also the Raman frequencies of ^{13}C-, (^{13}C + ^{15}N)-, ^{2}H-, and (^{2}H + ^{15}N)-Chl *a* and shifts upon the ^{15}N-substitution (in parentheses). Here again, the shifts by the ^{15}N-substitution

TABLE 1: Shifts upon the ^{15}N-Substitution and Assignments of the S_0 Raman Lines Obtained by Normal-Coordinate Analysis for NA-, ^{13}C-, and ^{2}H-Chl *a*

NA	^{15}N (Δ)	assignment	^{13}C	^{13}C + ^{15}N	assignment	^{2}H	^{2}H + ^{15}N	assignment
1668	1665 (−3)	C═O str	1624	1624 (0)	C═O str	1668	1668 (0)	C═O str
1608	1608 (0)	C_b-C_b str + C_a-C_m asym str	1575	1575 (0)	vinyl C═C str	1603	1603 (0)	C_b-C_b str
1552	1552 (0)	C_a-C_m asym str + C_b-C_b str	1552	1552 (0)	C_b-C_b str + C_a-C_m asym str	1594	1594 (0)	vinyl C═C str
1523	1523 (0)	C_a-C_m asym str + C_m-H def	1499	1497 (−2)	C_b-C_b str + C_a-C_m asym str	1573	1574 (+1)	C_b-C_b str
1486	1486 (0)	C_a-C_m sym str + C_a-C_b str	1478	1478 (0)	C_a-C_m asym str + C_m-H def	1539	1539 (0)	C_a-C_m asym str + C_b-C_b str
1437	1435 (−2)	Me deg def + C_a-C_m sym str	1444	1443 (−1)	C_a-C_m sym str + C_a-C_b str	1496	1496 (0)	C_a-C_m asym str
1388	1384 (−4)	C_a-N sym str	1399	1391 (−8)	C_a-C_m sym str + C_a-N asym str	1486	1487 (+1)	C_a-C_m sym str + C_a-C_b str
1376	1371 (−5)	C_a-N sym str	1365		C_a-C_b str + C_a-N asym str	1431	1427 (−4)	C_a-C_m sym str
1346	1340 (−6)	C_a-N sym str + C_m-H def	1343	1336 (−7)	C_a-N sym str	1415	1414 (−1)	C_a-N sym str + C_a-N asym str
1328	1326 (−2)	vinyl CH ip bends	1311	1306 (−5)	C_a-N sym str + C_m-H def	1364	1358 (−6)	C_a-N sym str
1303	1301 (−2)	C_m-H def	1303	1296 (−7)	C_a-N sym str + vinyl CH ip bends	1343	1337 (−6)	C_a-N sym str + C_a-C_b str
1287	1280 (−7)	C_m-H def + C_a-N sym str	1281	1279 (−2)	C_m-H def	1332		C_a-N asym str + C_a-N sym str
1261	1260 (−1)	C_a-C_b str + C_m-H def	1265	1258 (−7)	C_m-H def + C_a-N sym str	1319	1310 (−9)	C_a-N sym str
1211	1206 (−5)	ring V C−C str	1246	1242 (−4)	C_a-C_b str + C_m-H def	1238	1231 (−7)	C_a-N asym str + C−Me str
1184	1178 (−6)	vinyl CH ip bends + C_a-N asym str	1191	1189 (−2)	ring V C−C str	1208	1196 (−12)	C−Me str + C_a-N asym str
	1145	C_a-N asym str + ring V C−C str		1160	C_a-N asym str + ring V C−C str	1186		ring V C−C str + C_a-C_b str
1144	1131 (−13)	C−Me str + C_a-N asym str	1152	1145 (−7)	C_a-N asym str + vinyl CH ip bends	1164	1158 (−6)	$C_b''-C_b''$ str + C−Me str
1108	1105 (−3)	Me rock + C_a-N sym str	1131	1120 (−11)	C_a-N asym str + ring V C−C str	1138	1132 (−6)	Me sym def
1065	1063 (−2)	C_a-C_b str + Me rock		1112	C−Me str + C_a-N asym str	1123	1117 (−6)	Me sym def + C_a-N asym str
1046	1044 (−2)	ring V C−C str + Me rock	1108		C_a-N asym str + C_m-H def	1088		Me sym def
			1088	1084 (−4)	methylene CH_2 wag		1054	methylene CD_2 wag
			1063	1062 (−1)	Me rock + methylene CH_2 wag	1043	1039 (−4)	Me deg def + Me sym def
			1024	1022 (−2)	$C_b''-C_b''$ str			

lead us to the classification of the Raman lines into two groups, i.e., those that shift largely upon the ^{15}N-substitution and those that do not.

(c) Characterization of the S_1 Raman Spectra. Parts a-3 and a-4 of Figure 3 show the S_1 Raman spectra of NA- and ^{15}N-Chl *a*. The spectral pattern in the S_1 state is much simpler than that in the S_0 state. We can conclude that this difference in the number of observed Raman lines is not due to difference in the resonance conditions but due to difference in the molecular structure, because the $S_n \leftarrow S_1$ and the $S_n \leftarrow S_0$ absorption spectra are basically the same according to Shepanski and Anderson.[25] The simple spectral pattern in the S_1 state strongly suggests that the force constants within the C_a-C_m (C_a-N) group are very similar to one another and that only highly symmetric modes appear with high Raman intensity (vide supra). Another characteristic of the S_1 Raman spectra is the broadness of the observed Raman lines. This may be ascribed to Raman transitions from the higher vibrational levels in an anharmonic potential because the vibrational relaxation may not complete within 50 ps when the molecule was excited to higher electronic levels, which are responsible for the Soret absorption. Table 2 lists the S_1 Raman frequencies of NA- and ^{15}N-Chl *a* and shifts upon the ^{15}N-substitution (in parentheses). Here again, the effects of the ^{15}N-substitution lead us to a clear-cut classification of the Raman lines into two groups, i.e., those that shift only slightly (the 1589 and 1539 cm^{-1} lines, for example) and those that shift largely (the 1340 cm^{-1} line). Therefore, these three major Raman lines can be related to the highly symmetric C_b-C_b, C_a-C_m, and C_a-N stretching modes, respectively.

Parts b-3 and b-4 of Figure 3 show the S_1 Raman spectra of ^{13}C- and (^{13}C + ^{15}N)-Chl *a*. All the S_1 Raman lines are shifted to the lower frequencies by the ^{13}C-substitution, although the general spectral pattern of S_1 NA-Chl *a* is conserved. Here again, the classification of the Raman lines into two groups by the shifts upon the ^{15}N-substitution is clear: for example, the 1541 and 1491 cm^{-1} lines, which do not shift largely, can be associated with the C_b-C_b and the C_a-C_m stretchings, whereas the 1297 cm^{-1} line which shifts largely, can be associated with the C_a-N stretching. Parts C-3 and C-4 of Figure 3 show the S_1 Raman spectra of ^{2}H- and (^{2}H + ^{15}N)-Chl *a*. The 1585, 1537, and 1517 cm^{-1} Raman lines showing only small shifts upon the ^{15}N-substitution can be associated with the C_b-C_b and C_a-C_m stretchings, whereas the 1330 cm^{-1} Raman line showing much larger shifts can be associated with the C_a-N stretching. The frequencies of the S_1 Raman lines and shifts upon the ^{15}N-substitutions in various isotope species are summarized in Table 2.

(d) Characterization of the T_1 Raman Spectra. Parts a-5 and a-6 of Figure 3 show the T_1 Raman spectra of NA- and ^{15}N-Chl *a*. The spectral patterns in the T_1 state are completely different from those in the S_0 and S_1 states. Broad profiles consisting of very many split Raman lines appear in the 1650−1400 cm^{-1} region. The effects of the ^{15}N-substitution are also complicated in the set of Raman lines, and there are no distinct regions of the carbon−carbon stretchings and the carbon−nitrogen stretchings, for example. Actually, the 1538, 1502, and 1451 cm^{-1} Raman lines shift largely to the lower frequencies upon the ^{15}N-substitution, but the 1613, 1599, and 1560 cm^{-1} lines do not. The former three should be related to the C_a-N stretchings, whereas the latter three to the C_b-C_b and the C_a-C_m stretchings. The results strongly suggest that large increase in the C_a-N bond orders (relative to the C_b-C_b and C_a-C_m bond orders) takes place upon the S_0 to T_1 excitation. The Raman lines that are unaffected by the ^{15}N-substitution shift

TABLE 2: Characterization of the S_1 Raman Lines of NA and ^{13}C- and ^{2}H-Enriched Chl *a* Based on Shifts upon ^{15}N-Substitutions

NA	^{15}N (Δ)	assignment	^{13}C	$^{13}C + ^{15}N$ (Δ)	assignment	^{2}H	$^{2}H + ^{15}N$ (Δ)	assignment
1589	1591 (+2)	C_b-C_b str	1541	1543 (+2)	C_b-C_b str	1585	1582 (−3)	C_b-C_b str
1539	1539 (0)	C_a-C_m asym str + C_b-C_b str	1491	1489 (−2)	C_a-C_m asym str + C_b-C_b str	1537	1534 (−3)	C_a-C_m asym str + C_b-C_b str
1486		C_a-C_m sym str		1438	C_a-C_m asym str + C_a-C_m sym str	1517	1514 (−3)	C_a-C_m asym str
1434	1421 (−13)	C_a-N asym str + C_a-N sym str	1359		C_a-N sym str	1484		C_a-C_m sym str + C_a-C_b str
1383	1366 (−17)	C_a-N sym str	1297	1290 (−7)	C_a-N sym str + C_m-H def	1422		C_a-N sym str + C_a-N asym str
1340	1330 (−10)	C_a-N sym str + C_a-C_b str	1261		C_m-H def + C_a-N sym str	1330	1322 (−8)	C_a-N sym str + C_a-N asym str
1227	1217 (−10)	C_a-C_b str + C_m-H def	1195	1170 (−25)	C_a-C_b str + C_m-H def	1201	1180 (−21)	C−Me str + C_a-N asym str
1197	1187 (−10)	ring V C−C str	1163	1154 (−9)	vinyl CH ip bends + C_a-N asym str			
1117		C−Me str + C_a-N asym str						

TABLE 3: Characterization of the T_1 Raman Lines of NA and ^{13}C- and ^{2}H-Enriched Chl *a* Based on Shifts upon ^{15}N-Substitutions

NA	^{15}N (Δ)	assignment	^{13}C	$^{13}C + ^{15}N$ (Δ)	assignment	^{2}H	$^{2}H + ^{15}N$ (Δ)	assignment
1613	1616 (+3)	C_b-C_b str	1564	1565 (+1)	C_b-C_b str	1622	1621 (−1)	vinyl C=C str
1599	1601 (+2)	C_b-C_b str	1545	1545 (0)	C_b-C_b str	1589	1589 (0)	C_b-C_b str
1560	1561 (+1)	C_b-C_b str + C_a-C_m asym str	1509	1505 (−4)	C_a-C_m asym str + C_b-C_b str	1542	1542 (0)	C_a-C_m asym str + C_b-C_b str
1538	1531 (−7)	C_a-N sym str + C_m-H def	1486	1490 (+4)	C_a-N sym str + C_m-H def	1497	1490 (−7)	C_a-C_b str + C_a-C_m asym str
1502	1497 (−5)	C_a-N sym str + C_a-C_m asym str	1457	1458 (+1)	Me deg def	1445	1443 (−2)	C_a-N asym str
1451	1446 (−5)	C_a-C_m asym str + C_a-N asym str	1438	1438 (0)	C_a-C_m sym str + C_a-C_b str	1317	1308 (−9)	C_a-N sym str
1414	1417 (+3)	vinyl CH ip bends	1402	1401 (−1)	vinyl CH ip bends	1199	1192 (−7)	C−Me str + C_a-N asym str
1337		C_a-N sym str + C_m-H def	1378	1370 (−8)	C_a-N asym str + C_a-C_m asym str	1170	1167 (−3)	$C_b''-C_b''$ str
1307	1307 (0)	C_m-H def	1284	1274 (−10)	C_m-H def + C_a-N sym str	1141	1139 (−2)	Me sym def + C−Me str
1239	1235 (−4)	C_m-H def + C_a-N sym str	1210	1206 (−4)	C_a-C_b str + C_m-H def		1109	Me sym def + ring V C−C str
1198	1194 (−4)	C_a-N asym str + vinyl CH ip bends	1113	1108 (−5)	ring V C−C str + C_a-N asym str	1052	1053 (+1)	methylene CD_2 wag
1138		C−Me str + Me rock	1079	1074 (−5)	C_a-N asym str + C−Me str	1036	1032 (−4)	Me deg def + Me sym def
1104	1099 (−5)	C−Me str + C_a-N asym str						

to the higher frequencies on going from the S_0 to the T_1 state, a result that suggests increase in the carbon−carbon bond orders as well.

Parts b-5 and b-6 of Figure 3 show the T_1 Raman spectra of ^{13}C- and ($^{13}C + ^{15}N$)-Chl *a*. Upon the ^{13}C-substitution, all the spectral profiles are shifted to the lower frequencies, keeping the overall spectral pattern of T_1 NA-Chl *a*. However, the order of the classified Raman lines by the ^{15}N shifts is changed in T_1 ^{13}C-Chl *a*: the 1509, 1486, and 1378 cm^{-1} Raman lines shift largely, whereas the 1564, 1545, 1457, 1438, and 1402 cm^{-1} Raman lines do not. Parts c-5 and c-6 of Figure 3 show the T_1 Raman spectra of ^{2}H- and ($^{2}H + ^{15}N$)-Chl *a*. Because of the shifts of the C−H and C_m-H ip bendings to the lower frequencies, the coupling patterns are completely changed, and the carbon−carbon and carbon−nitrogen stretching vibrations in the low-frequency region give rise to much clearer spectral patterns. Upon the additional ^{15}N-substitution, the 1497 and the 1317 cm^{-1} Raman lines shift clearly, and the rest of the Raman lines in the high-frequency region remain unaltered. The results indicate another ordering of the classified Raman lines. The frequencies of the T_1 Raman lines and shifts upon the ^{15}N-substitution in various isotope species are summarized in Table 3.

Figure 4 (indicated as "obs") depicts the classification of the S_0, S_1, and T_1 Raman lines (1700−1300 cm^{-1} region) by the shifts upon the ^{15}N-substitution for the NA-, ^{13}C-, and ^{2}H-Chl *a*; those that shift more than 4 cm^{-1} are shown by the broken lines, and those that do not are shown by the solid lines.

The Procedure of Normal-Coordinate Analysis. The normal-coordinate analyses were performed on the basis of the general consideration of the normal modes and the characterization of the S_0, S_1, and T_1 Raman spectra, which have been described in the previous section. The calculations of the normal vibrations were performed only for the ip modes by the use of a molecular model shown in Figure 1b (see the Experimental Section for the details).

Since the number of calculated normal modes is much larger than the number of observed Raman lines, the following criteria (assumptions) were used in correlating the calculated normal modes to the observed Raman lines: (1) Those Raman lines that shift largely upon the ^{15}N-substitution should be related to the C_a-N stretchings, whereas those that do not should be related to the carbon−oxygen and carbon−carbon stretchings or the carbon−hydrogen ip bendings (deformations). (2) The C_a-C_m asymmetric stretchings couple strongly with the C_m-H ip bendings, and therefore, they should exhibit large low-frequency shifts upon the ^{2}H-substitution. (3) Peripheral modes should not give rise to high Raman intensity except for the C=O stretching, the C_m-H and the vinyl C−H ip bendings, and the ip deformations of the methyl and methylene groups directly attached to the chlorin skeleton. (4) Those skeletal modes whose displacements of atoms are extended over a wide region of the macrocycle, and at the same time, exhibit the pseudo C_{2v} symmetry, should give rise to high Raman intensity. Criterion 4 may hold true under most of the preresonance conditions, but it does not necessarily hold under the rigorous-resonance condition where those vibrational modes, in which the displacements of atoms are in accord with the structural change upon the particular electronic excitation in resonance, generally give rise to the highest Raman intensity.

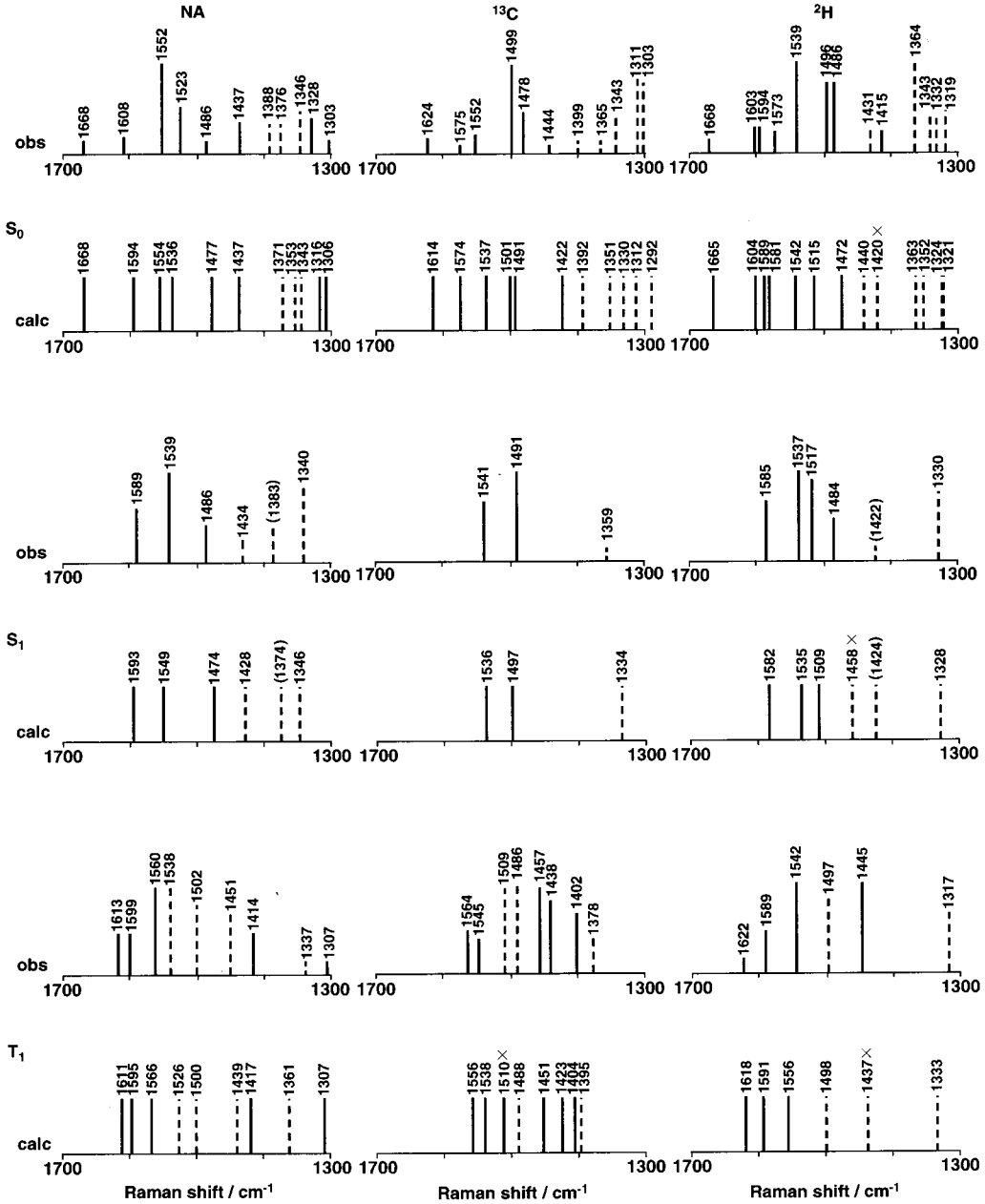

Figure 4. Classification of the observed Raman lines (indicated as "obs") in the S_0, S_1, and T_1 states into two groups: those that shift more than 4 cm^{-1} upon the $^{14}N \rightarrow {}^{15}N$ substitution are shown in broken lines, whereas those do not are shown in solid lines. Classification of the calculated frequencies of Raman active modes (indicated as "calc"): those that shift more than 3 cm^{-1} upon the $^{14}N \rightarrow {}^{15}N$ substitution are shown in broken lines, and those do not are shown in solid lines for comparison. Calculated frequencies that do not realize the observed classification are marked by $\times$.

In the normal-coordinate analysis in the S_0 state, the UBS force constants as well as the non-UBS stretching−stretching and bending−bending cross-terms were transferred, as a initial set, from those of Ni-OEP,[23] β-carotene,[26] retinal,[27] and hydrocarbons including ethene, propene, isobutane, and polyethylene.[28] Because of the limited number of observed Raman lines, we adjusted only the following set of force constants (29 in total): (1) the C_b-C_b, C_a-C_m, C_a-C_b, and C_a-N stretchings in the conjugated part of the chlorin skeleton, the C═O and the vinyl C═C stretchings, and the skeletal C−C stretchings, (2) a part of the C−C−H and the vinyl C−H bendings, and (3) some of the non-UBS cross-terms, i.e., $(C_a-C_m)(C_a-C_m)$, $(C_a-N)(C_a-N)$, $(C_a-C_m)(C_a-C_b)$ and $(C_a-C_m)(C_a-N)$.

In the adjustment of the S_0 force constants, we first used the Raman lines of the NA-Chl *a*, ^{13}C-labeled Chl *a*, and ^{2}H-Chl *a* for rough adjustment, and then, further refinement was done by the use of the shifts upon additional ^{15}N-substitutions. The adjustment of the C_a-C_m and the C_a-N stretching force constants in the S_1 and T_1 states (eight each) was performed to realize the classification of the Raman lines by the shifts upon the ^{15}N-substitution for NA-, ^{13}C-, and ^{2}H-Chl *a* (Figure 4, obs). In the T_1 state, it was necessary to remove the constraint on these stretching force constants, i.e., $C_a-C_m > C_a-N$. The adjustment was based on the assumption that all the rest of the force constants were the same as those in the S_0 state and that the sum of the stretching force constants over the total conjugated system should not be changed so drastically, because only one electron out of the 24 π-electrons in the total conjugated system is transferred to an upper electronic level upon excitation.

Characterization of the Raman-Active Modes and Changes in the C_a-C_m and the C_a-N Bond Orders upon Singlet and

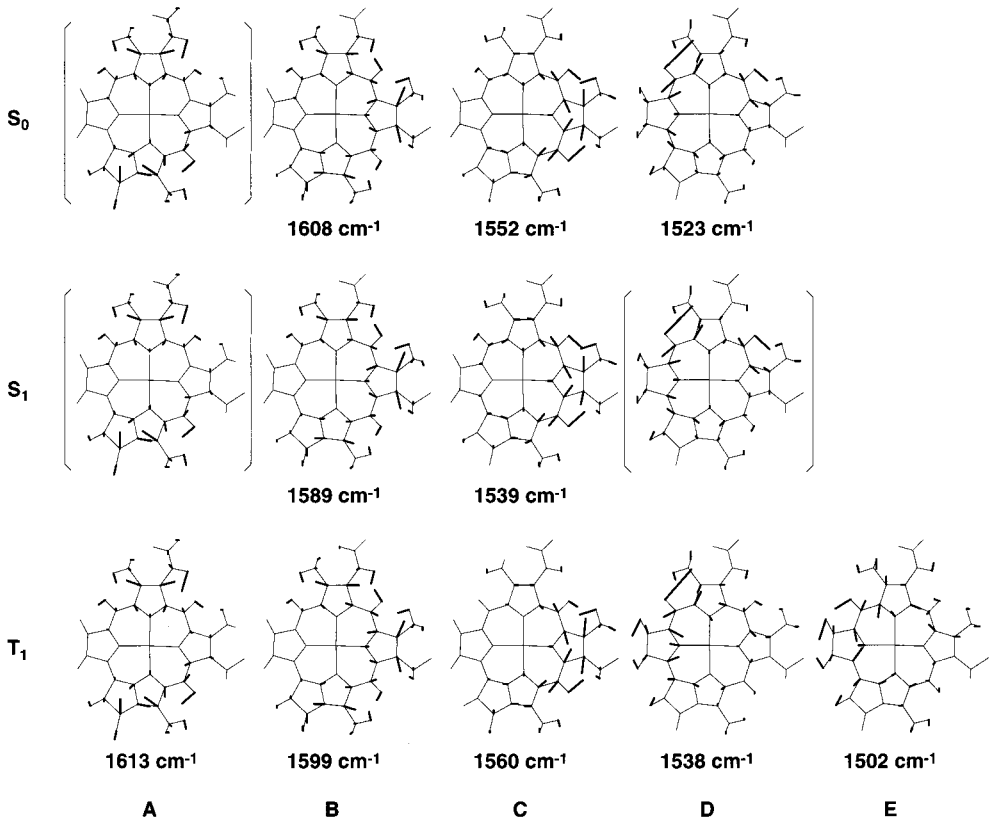

Figure 5. Normal modes (A−E) responsible for the S_0, S_1, and T_1 Raman lines in the 1650−1500 cm^{-1} region. Those modes that were not detected, at least under the present resonance conditions, are shown in square brackets.

Triplet Excitation. *(a) Classification of the S_0, S_1, and T_1 Raman Lines by the Shifts upon the ^{15}N-Substitution Calculated after the Adjustment of the Force Constants.* Figure 4 (indicated as "calc") shows the calculated classification of the Raman lines (1700−1300 cm^{-1} region) by the shifts upon the ^{15}N-substitution for NA-, ^{13}C-, and ^{2}H-Chl *a* in the S_0, S_1, and T_1 states; the broken lines show those vibrational modes that shift more than 3 cm^{-1} upon the ^{15}N-substitution, whereas the solid lines show those that do not. The observed ordering of the classified Raman lines is nicely realized by the calculated ordering in all of NA-, ^{13}C-, and ^{2}H-Chl *a* in the three different electronic states. The calculated modes which do not satisfy the classification are marked by ×; they appear at 1420 cm^{-1} in S_0 ^{2}H-Chl *a*, at 1458 cm^{-1} in S_1 ^{2}H-Chl *a*, at 1510 cm^{-1} in T_1 ^{13}C-Chl *a*, and 1437 cm^{-1} in T_1 ^{2}H-Chl *a*. The merit of correct prediction is 69/73 = 0.95. The averaged discrepancy between the observed and the calculated frequencies was 8, 8, 7 cm^{-1} in the S_0, S_1, and T_1 states, respectively. (We actually focused on realizing the ordering of the classified Raman lines rather than fitting the calculated to the observed frequency for each Raman line.) The results show that our general considerations and assumptions that were made before the normal-coordinate analysis are reasonable, and the sets of force constants that have been determined are fairly reliable.

(b) Assignments of the S_0, S_1, and T_1 Raman Lines. Table 1 lists the assignments of the S_0 Raman lines for NA-, ^{15}N-, ^{13}C-, (^{13}C + ^{15}N)-, ^{2}H-, and (^{2}H + ^{15}N)-Chl *a* which were obtained as the results of the normal-coordinate analysis: In NA-, ^{15}N-, ^{13}C-, and (^{13}C + ^{15}N)-Chl *a*, the normal vibrations actually appear in the following order: the C═O and the vinyl C═C stretchings, the C_b-C_b stretchings, the C_a-C_m asymmetric stretchings, the C_a-C_m symmetric stretchings, the C_a-N symmetric stretchings, the vinyl CH ip bendings, the C_m-H ip deformations, the C_a-N asymmetric stretchings, the CH_2 and CH_3 rockings, and other carbon−carbon single-bond stretchings. In ^{2}H- and (^{2}H + ^{15}N)-Chl *a*, the ^{2}H-substituted methyl, methylene, and methine deformation vibrations shift below 1200 cm^{-1}, and almost pure stretching vibrations appear on the higher frequency side.

Table 2 lists the assignments of the S_1 Raman lines for the same set of isotope species: The general order of the stretching vibrations in the S_0 state is conserved, but only the highly symmetric vibrational modes are observed as strong Raman lines. The C_a-N stretching mode shifts to the higher frequencies leaving the C_a-C_b and other carbon−carbon stretching vibrations in the lower frequency region. The peripheral local modes as well as less symmetric skeletal modes do not give rise to appreciable Raman intensity, which simplifies the spectral patterns.

Table 3 lists the assignments of the T_1 Raman lines for the set of isotope species: In NA-, ^{15}N-, ^{13}C-, and (^{13}C + ^{15}N)-Chl *a*, complicated couplings among the C_a-C_m stretchings, the C_m-H deformations, and the upshifted C_a-N stretchings cause completely different patterns of vibrational modes in the 1700−1300 cm^{-1} region. In the case of ^{2}H- and (^{2}H + ^{15}N)-Chl *a*, however, the vibrational modes become much better defined because of the shifts of the carbon−deuterium ip deformation vibrations below 1000 cm^{-1}; the carbon−carbon single-bond stretchings as well as the ^{2}H-substituted methyl and methylene rockings actually appear in the 1200−1000 cm^{-1} region. All the above results of the normal-coordinate analysis confirm the general consideration of the vibrational modes and the characterization of the S_0, S_1, and T_1 Raman lines described in the preceding section.

(c) Comparison of the Skeletal Modes Giving Rise to the Raman Lines in the High-Frequency Region. Figure 5 shows the normal modes that potentially give rise to Raman lines in the 1650−1500 cm^{-1} region. (1) Mode A is basically the C_b-

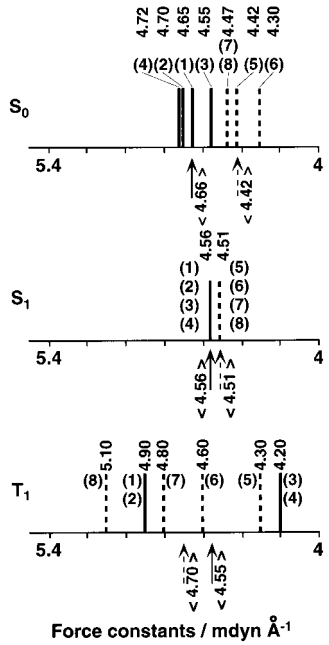

Figure 6. Values of the C_a-C_m stretching force constants (shown in solid lines) and those of the C_a-N stretching force constants (shown in broken lines) in the S_0, S_1, and T_1 states, which have been determined by the present normal-coordinate analyses. The numbers in parentheses refer to the positions of the C_a-C_m and the C_a-N bonds shown in Figure 1b; the averaged force constants for the C_a-C_m and the C_a-N bonds are also shown in brackets.

C_b stretchings in rings I and III which are coupled out-of-phase with respect to the pseudo-C_2 axis, whereas mode B is the C_b-C_b stretchings on rings I, II, and III coupled in-phase; more specifically, coupling with the C═O stretching is seen in the former, and coupling with the C_a-C_m stretchings is seen in the latter. Symmetrically, only mode B is supposed to give rise to high Raman intensity; however, mode A also appears in the T_1 Raman spectrum. (2) Mode C is the C_a-C_m asymmetric stretchings and the C_m-H ip deformations coupled in-phase with respect to the pseudo C_2 axis; this mode takes place on the ring II side and couples with the C_b-C_b stretching. This mode gives rise to very high Raman intensity in all the electronic states owing to higher symmetry and to higher contributions of the skeletal stretchings. Mode D is another type of the C_a-C_m asymmetric stretchings on the ring IV side coupled with the C_m-H ip deformation. This mode is weaker in the S_0 Raman spectrum owing to the absence of the contribution of the conjugated C_b-C_b stretching; it is not clearly seen in the S_1 Raman spectrum, but it gets stronger in the T_1 state. (3) Mode E has higher contribution of the C_a-N stretching, which uniquely appears in the T_1 Raman spectrum. It is to be noted that similar types of vibrational modes are taking place in this spectral region for all the different electronic states and that changes in the vibrational modes originating from changes in the stretching force constants and changes in the molecular geometry upon the resonant electronic transition give rise to the large changes in Raman frequencies and intensities.

(d) Changes in the C_a-C_m and C_a-N Bond Orders upon Singlet and Triplet Excitation As Determined by Sets of Stretching Force Constants. Figure 6 shows the C_a-C_m (solid lines) and the C_a-N (broken lines) stretching force constants in the S_0, S_1, and T_1 states that were determined in the present normal-coordinate analysis. The numbers in parentheses refer to the positions of the C_a-C_m and the C_a-N bonds shown in Figure 1b. The S_0, S_1, and T_1 force constants shown in Figure 6 can be characterized as follows: In the S_0 state, both the C_a-C_m and the C_a-N stretching force constants are slightly dispersed. The former ones are definitely larger than the latter ones, the average values being 4.66 and 4.42 mdyn·Å^{-1}, respectively. In the S_1 state, each of the C_a-C_m and the C_a-N stretching force constants takes one and the same value. The C_a-C_m stretching force constant (4.56 mdyn·Å^{-1}) is slightly larger than the C_a-N stretching force constant (4.51 mdyn·Å^{-1}); the difference is decreased appreciably in comparison to that in the above averaged values in the S_0 state. In the T_1 state, the C_a-C_m stretching force constants are largely split into two groups, one is higher and the other is definitely lower than those force constants in the S_0 state. On the other hand, the C_a-N force constants are split apart into four. Here, the average value of the C_a-N force constants (4.70 mdyn·Å^{-1}) is larger than that of the C_a-C_m force constants (4.55 mdyn·Å^{-1}). The results indicate that large reorganization of the bond orders takes place in the chlorin skeleton upon triplet excitation and that the inversion of the C_a-C_m and C_a-N bond orders takes place as the averaged values. However, the absolute value of each force constant in the S_0 and T_1 states is of limited significance because of the assumption of C_2 symmetry for the C_a-C_m and C_a-N stretching force constants (vide supra).

Discussion

Analysis of the S_0 Raman Spectrum. Extensive efforts have been made to analyze the S_0 Raman spectrum of Chl *a*: (1) Lutz[29] proposed a set of empirical assignments of Raman lines on the bases of their shifts upon the $^{14}N \rightarrow {}^{15}N$ and $^{24}Mg \rightarrow {}^{25}Mg$ substitutions and of spectral comparison of Chl *a* with its derivatives having various peripheral groups. Reference was also made to the normal-coordinate analysis of Ni-OEP[23] as well as the results of resonance-Raman excitation-profile measurements.[29] (2) Tasumi and Fujiwara[30] found coordination-marker Raman lines to distinguish the penta- and hexacoordinated states. To establish the expansion of the 16-membered ring on going from the penta- to the hexacoordinated state, the effects of the central-metal substitutions on the C_a-C_m stretching frequency were examined. Empirical assignments of the Raman lines were also proposed by means of the partial and specific $^1H \rightarrow {}^2H$ substitutions of Zn methylpyropheophorbide *a*. (3) Bocian and co-workers[31] performed a normal-coordinate analysis of model compounds of Chl *a* by the use of QCFF/PI method and showed systematic changes in the normal modes upon degradation of molecular symmetry from Ni-OEP toward Chl *a*.

The assignments of the three coordination-marker Raman lines at 1608 (w), 1552 (s), and 1523 (m) cm^{-1} (modes B, C, and D) obtained in the present investigation are slightly different from those of the corresponding Raman lines at 1615 (w), 1560 (s), and 1530 (m) cm^{-1} (measured at 30 K by Lutz[29]) given by the above investigators: Lutz[29] assigned these three Raman lines to the C_a-C_m, C_b-C_b, and ($C_b-C_b + C_a-C_b$) stretchings, respectively; Tasumi and Fujiwara[30] to the C_a-C_m, C_a-C_m, and ($C_a-C_m + C_b-C_b$) stretchings, respectively; and Boldt et al.[31] to the C_a-C_m, ($C_a-C_b + C_b-C_b$), and ($C_b-C_b + C_a-C_b$) stretchings, respectively. In all of the above cases, the weak Raman line with the highest frequency was associated with the C_a-C_m stretching vibration. This assignment explains nicely the observation by Fujiwara and Tasumi that the frequency of this mode is most sensitive to the central metal (the core size), although the strong and medium Raman lines appearing in the lower-frequency region are also sensitive to the core size because of the conjugation effects.

On the contrary, the results of the present normal-coordinate analysis (see the L_x matrix in Figure 5) shows that the C_b-C_b,

C_a-C_m (asym), and C_a-C_m (asym) stretchings contribute most in these normal modes giving rise to the 1608 (w), 1552 (s), and 1523 (m) Raman lines, respectively. The results originate from the following correlations of the observed Raman lines used in the present normal-coordinate analysis: We correlated the 1552 and 1523 cm^{-1} Raman lines of NA-Chl *a* to the 1539 and 1496 cm^{-1} Raman lines of ^{2}H-Chl *a*, and then the shifts upon the ^{2}H substitution turns out to be 13 and 27 cm^{-1}. Since the C_a-C_m asymmetric stretching couple with the neighboring C_m-H ip bending and exhibits much larger low-frequency shift than the C_b-C_b stretching upon the ^{2}H substitution (as has been established in the cases of Ni-OEP[24] and Ni-OEC[32]), we associated the above pair of Raman lines to the C_a-C_m asymmetric stretchings in order to explain their large deuteration shifts. The 1608 cm^{-1} Raman line of NA-Chl *a* shifts to the 1603 cm^{-1} Raman line of ^{2}H-Chl *a*, the shift upon ^{2}H substitution being 5 cm^{-1}; therefore, this Raman line can be associated with the C_b-C_b stretching. All the attempts to associate the 1608 cm^{-1} Raman line to the asymmetric C_a-C_m stretching failed to explain the observed ^{2}H-substitution shifts of the major 1552 cm^{-1} Raman line. Further investigation is necessary to fully establish the assignments of those three Raman lines.

Changes in Bond Orders upon Triplet Excitation: Comparison among the Linear and Cyclic Conjugated Systems. "The triplet-excited region" where large changes in bond order take place was first identified in the linear conjugated chains of retinoids and carotenoids (see refs 8 and 33 for reviews). In this triplet-excited region, a double bond becomes more single bond-like, whereas a single bond becomes more double bond-like. It is localized in the central part of the conjugated chain, and it has a span of approximately six conjugated double bonds.

In retinal, the changes in bond order in the conjugated chain were determined in terms of a set of carbon−carbon and carbon−oxygen stretching force constants in both the S_0 and T_1 states:[9] upon triplet excitation, the C7═C8, C9═C10, C11═C12, C13═C14, and C15═O stretching force constants decrease (6.40 → 5.90, 6.35 → 5.53, 6.27 → 5.17, 6.50 → 6.30, and 9.73 → 8.74 mdyn·Å^{-1}), whereas the C8−C9, C10−C11, and C12−C13 stretching force constants increase (3.96 → 4.60, 4.49 → 4.91 and 4.13 → 4.43 mdyn·Å^{-1}). The decrease in the C═C bond orders could be recognized, at a glance, by the downshift of the strongest, in-phase C═C stretching Raman line (1582 → 1553 cm^{-1}) upon triplet excitation. However, the increase in the C−C bond order was not easily recognized by spectral comparison, because of the strong coupling of the C−C stretchings with the C−H ip deformations.

In spheroidene, the changes in the bond order upon triplet excitation in the central part of the conjugated chain are now being determined in terms of stretching force constants in the S_0 and T_1 states (Y. Mukai, M. Abe, R. Fujii, R. Gebhard, J. Lugtenburg, and Y. Koyama, unpublished results); the C9═C10, C11═C12, and C13═C14 stretching force constants decrease (6.30 → 6.00, 5.99 → 5.51, and 5.92 → 5.41 mdyn·Å^{-1}), whereas the C10−C11, C12−C13, C14−C15, and C15′−C14′ stretching force constants increase (4.30 → 4.33, 4.30 → 4.48, 4.25 → 4.35, and 4.30 → 4.39 mdyn·Å^{-1}). The decrease in the C═C bond orders upon triplet excitation could be easily recognized by the downshift of the strongest, in-phase C═C stretching Raman line (1529 → 1500 cm^{-1}).

Large changes in bond order upon triplet excitation have been found in cyclic conjugated systems as well: Table 4 lists the frequencies of the C_a-C_m stretching Raman lines in the S_0 and T_1 states of bacteriochlorin, octaethylchlorin, and octaethylporphyrin rings. The C_a-C_m stretching frequencies, or an averaged value of them, downshifts systematically upon triplet excitation in each of the compounds. Therefore, the apparent decrease in bond order upon triplet excitation in the C_a-C_m bonds having a double-bond character parallels to the cases of the C═C bonds in the above linear conjugated chains. Unfortunately, the excited-state force constants have not been determined yet for the above set of compounds (as far as the authors know).

TABLE 4: Shifts of the C_a-C_m Stretching Raman Lines upon the $S_0 \rightarrow T_1$ Excitation Showing Decrease in Bond Orders in the Macrocycle

molecule	S_0 state	T_1 state	difference
BChl *a*[a]	1611, 1463 (avg. 1537)	1587, 1409 (avg. 1498)	(−39)
BPhe *a*[b]	1612, 1586, 1465 (avg. 1554)	1587, 1551, 1451 (avg. 1530)	(−24)
ZnOEC[c]	1616, 1486 (avg. 1551)	1597, 1464 (avg. 1531)	(−20)
ZnOEP[d]	1486	1450	(−36)
CuOEP[e]	1505	1468	(−37)
NiOEP[f]	1655, 1603 (avg. 1629)	1627, 1562 (avg. 1595)	(−34)
NiOEP[g]	1657, 1520 (avg. 1589)	1629, 1494 (avg. 1562)	(−27)

[a] Reference 14. [b] Reference 13. [c] Reference 34. [d] Reference 35. [e] Reference 36. [f] Reference 37. [g] Reference 38.

In the case of BChl *a*, a closest analogue of Chl *a*, both the low-frequency shift of the in-phase C_a-C_m stretching Raman line that appears in the higher frequency region as well as the high-frequency shifts of a group of the C_a-N stretching Raman lines that appears in the lower-frequency region were observed upon triplet excitation; the C_a-N stretching Raman lines in the middle were not affected (see Figure 5 of ref 14). The results indicate that the C_a-C_m bonds having a double-bond character decrease in bond order, whereas the C_a-N bonds having a single-bond character increase in bond order. Similar changes were found upon triplet excitation of BPhe *a* as well.[15]

In the present compound of Chl *a*, the changes in the C_a-C_m and the C_a-N bond orders upon triplet excitation could be extracted only in terms of a set of stretching force constants shown in Figure 6, because the S_0 and T_1 Raman spectra are so complicated. The drastic changes in the carbon−carbon and carbon−nitrogen bond orders upon triplet excitation and the resultant strong coupling between the C_a-C_m and the C_a-N stretching vibrations make it extremely difficult to pick out any T_1 Raman line that can be correlated with the C_a-C_m bond order, for example. This drastic reorganization of the electronic and molecular structure may originate from the fact that "the triplet-excited region" is packed within a small region consisting of the 16-membered ring and three pyrrole rings I, II, and III. The C_b-C_b double bond in ring II of the chlorin skeleton seems to have a strong effects in the T_1 state because the systematic changes in bond order are seen in the case of the bacteriochlorin skeleton upon triplet excitation.

Conclusions

The following answers to the questions addressed in the Introduction section have been obtained. (1) What kind of changes in bond order take place in the chlorin skeleton upon singlet and triplet excitation? The C_a-C_m and C_a-N stretching force constants determined in the present investigation have lead us to the following conclusions: In the S_0 state, the C_a-C_m bond orders are higher than the C_a-N bond orders, and weak positional dependence is seen in both of them. Upon excitation to the S_1 state, the C_a-C_m bond orders decrease, whereas the C_a-N bond orders increase; both of them converge into a single value. Upon excitation to the T_1 state, drastic reorganization of the bond orders takes place in the macrocycle, i.e., the C_a-

C_m bond orders split into two and the C_a-N bond orders split into four. The averaged C_a-N bond order becomes larger than the averaged C_a-C_m bond order. (2) How do the above changes in the bond orders upon excitation compare with, or contrast to, those of other cyclic conjugated systems including BChl *a* and metal octaethylporphyrins and octaethylchlorins and those of the linear conjugated systems including retinoids and carotenoids? Changes in bond order upon *triplet* excitation have been characterized as follows: In linear conjugated systems, the bond orders of the carbon−carbon double bonds decrease and those of the carbon−carbon single bonds increase in the triplet-excited region, which is located in the central part of the conjugated chain. In metal octaethylporphyrins and octaethylchlorins, the bond orders of the C_a-C_m bonds with a double-bond character decrease, but the changes in the C_a-N bond orders are not clear. In BChl *a*, the bond orders of the C_a-C_m bonds having a double-bond character decrease, whereas those of the C_a-N bonds having a single-bond character increase. The changes in the bond orders in the present compound, Chl *a*, are very unique in the sense that there are no clear differences in bond order between the C_a-C_m and the C_a-N bonds in the T_1 state and that inversion of bond orders takes place upon triplet excitation as averaged values.

Acknowledgment. The authors thank Mr. Wataru Maruyama of SHOKO Co. Ltd. and Chlorella Industries, Inc. for the gifts of ($^{13}C + {}^{15}N$)- and ($^{2}H + {}^{15}N$)-Chl *a*. They are grateful to Dr. Leenawaty Limantara for reading the manuscript. This work has been supported by a grant-in-aid from the Ministry of Education, Science, Sports and Culture, Japan (6239101).

References and Notes

(1) Deisenhofer, J.; Norris, J. R. *The Photosynthetic Reaction Center*; Academic Press: New York, 1993; Vols. 1 and 2.

(2) Frank, H. A.; Violette, C. A. *Biochim. Biophys. Acta* **1989**, *976*, 222.

(3) Krauss, N.; Schubert, W.-D.; Klukas, O.; Fromme, P.; Witt, H. T.; Saenger, W. *Nature Struct. Biol.* **1996**, *3*, 965.

(4) Satoh, K. *The Photosynthetic Reaction Center*; Academic Press: New York, 1993; Vol. 1, p 289.

(5) Petke, J. D.; Maggiora, G. M.; Shipman, L. L.; Christoffersen, R. E. *J. Mol. Spectrosc.* **1978**, *73*, 311.

(6) Petke, J. D.; Maggiora, G. M.; Shipman, L.; Christoffersen, R. E. *Photochem. Photobiol.* **1979**, *30*, 203.

(7) Petke, J. D.; Maggiora, G. M.; Shipman, L. L.; Christoffersen, R. E. *Photochem. Photobiol.* **1980**, *32*, 399.

(8) Koyama, Y.; Mukai, Y. *Advances in Spectroscopy Vol. 21: Biomolecular Spectroscopy Part B*; Wiley: New York, 1993; Chapter 2.

(9) Mukai, Y.; Abe, M.; Katsuta, Y.; Tomozoe, S.; Ito, M.; Koyama, Y. *J. Phys. Chem.* **1995**, *99*, 7160.

(10) Nishizawa, E.; Koyama, Y. *Chem. Phys. Lett.* **1990**, *172*, 317.

(11) Nishizawa, E.; Hashimoto, H.; Koyama, Y. *Chem. Phys. Lett.* **1991**, *181*, 387.

(12) Koyama, Y.; Limantara, L.; Nishizawa, E.; Misono, Y.; Itoh, K. In *Proceedings of 7th International Conference on Time-Resolved Vibrational Spectroscopy VII*; Los Alamos National Laboratory: Santa Fe, NM, 1995; p 45.

(13) Koyama, Y.; Limantara, L. *Spectrochim. Acta*, in press.

(14) Limantara, L.; Katheder, I.; Scheer, H.; Schäfer, W.; Koyama, Y. *Chem. Phys. Lett.* **1996**, *262*, 656.

(15) Limantara, L. Ph.D. Dissertation, Kwansei Gakuin University, 1998.

(16) Nishizawa, E.; Hashimoto, H.; Koyama, Y. *Chem. Phys. Lett.* **1989**, *164*, 155.

(17) Kanzaki, M.; Yuzawa, T.; Hiura, H.; Takahashi, H. *Chem. Phys. Lett.* **1990**, *169*, 85.

(18) Omata, T.; Murata, N. *Plant Cell Physiol.* **1983**, *24*, 1093.

(19) Harris, E. H. *Chlamydomonas Sourcebook*; Academic Press: New York, 1989.

(20) Watanabe, A. *J. Gen. Appl. Microbiol.* **1960**, *6*, 283.

(21) Chow, H.-C.; Serlin, R.; Strouse, C. E. *J. Am. Chem. Soc.* **1975**, *97*, 7230.

(22) Shimanouchi, T. *Computer Programs for Normal Coordinate Treatment of Molecules*; University of Tokyo: Tokyo, 1968.

(23) Abe, M.; Kitagawa, T.; Kyogoku, Y. *J. Chem. Phys.* **1978**, *69*, 4526.

(24) Li, X.-Y.; Czernuszewicz, R. S.; Kincaid, J. R.; Stein, P.; Spiro, T. G. *J. Phys. Chem.* **1990**, *94*, 47.

(25) Shepanski, J. F.; Anderson, R. W., Jr. *Chem. Phys. Lett.* **1981**, *78*, 165.

(26) Saito, S.; Tasumi, M. *J. Raman Spectrosc.* **1983**, *14*, 310.

(27) Saito, S.; Tasumi, M. *J. Raman Spectrosc.* **1983**, *14*, 236.

(28) Mizushima, S.; Shimanouchi, T. *The Infrared Absorption and the Raman Effect*; Kyouritsu: Tokyo, 1958.

(29) Lutz, M. *Advances in Infrared and Raman Spectroscopy*; Wiley: New York, 1984; Vol. 11, Chapter 5.

(30) Tasumi, M.; Fujiwara, M. *Spectroscopy of Inorganic-Based Materials*; Wiley: New York, 1987; Chapter 6.

(31) Boldt, N. J.; Donohoe, R. J.; Birge, R. R.; Bocian, D. F. *J. Am. Chem. Soc.* **1987**, *109*, 2284.

(32) Prendergast, K.; Spiro, T. G. *J. Phys. Chem.* **1991**, *95*, 1555.

(33) Koyama, Y.; Mukai, Y.; Kuki, M. *Laser Spectroscopy of Biomolecules, 4th International Conference on Laser Applications in Life Sciences*, Proceedings of SPIE−The International Society for Optical Engineering, Jyvaskyla, Finland, 1992; SPIE: Bellingham, WA, 1993; Vol. 1921, p 191.

(34) Blackwood, M. E., Jr.; Kumble. R.; Spiro, T. G. *J. Phys. Chem.* **1996**, *100*, 18037.

(35) Kreszowski, D. H.; Deinum, G.; Babcock, G. T. *J. Am. Chem. Soc.* **1994**, *116*, 7463.

(36) Asano-Someda, M.; Aoyagi, K.; Kitagawa, T. *Chem. Phys. Lett.* **1996**, *257*, 492.

(37) Apanasevich, P. A.; Kvach, V. V.; Orlovich, V. A. *J. Raman Spectrosc.* **1989**, *20*, 125.

(38) Kruglik, S. G.; Mizutani, Y.; Kitagawa, T. *Chem. Phys. Lett.* **1997**, *266*, 283.